Tribol Lett (2011) 43:185–195
DOI 10.1007/s11249-011-9793-7

ORIGINAL PAPER

Measurement and Characterization of "Resonance Friction" at High Sliding Speeds in a Model Automotive Wet Clutch

Xavier Banquy · Daniel D. Lowrey · Nataly Belman · Younjin Min · Gregory Mordukhovich · Jacob N. Israelachvili

Received: 9 November 2010 / Accepted: 28 April 2011 / Published online: 17 May 2011
Springer Science+Business Media, LLC 2011

Abstract The friction forces between various lubricated "friction materials" and sapphire disks were measured using a new "high-speed" rotating disk attachment to the surface forces apparatus (SFA). Two different clutch lubricants and two different friction materials were tested at sliding speeds and normal loads from 5 to 25 m/s, and 0.2 to 1 N (nominal pressures $\sim$1 MPa), respectively. The results show that "resonance friction"—characterized by large amplitude *oscillatory* (i.e., sinusoidal) vibrations, also known as shudder or chatter—dominates dynamical considerations at high sliding speed, replacing the smooth sliding or low-amplitude stick–slip that is characteristic of low speed/low load sliding. The characteristic (rotational) speeds or frequencies at which resonance friction occurs depend only on the coupled/uncoupled mechanical resonance frequencies of the loading and friction-sensing mechanisms. In contrast, the *intensity* of and *time* to enter/exit shudder depends strongly on the lubricating oil and, to a lesser extent, on the friction material. Physical–chemical analyses of the friction materials before and after testing showed that the samples undergo primarily structural rather than chemical changes. Our results provide new fundamental insights into the resonance friction phenomenon and suggest means for its control.

Keywords Clutch lubrication · Shudder · Chatter · Resonance friction · Wear

1 Introduction

A large number of industrial systems are designed to work under tribologically "extreme conditions" of high sliding speeds ranging from cm/s to several tens of m/s, over a large range of loads (pressures). Friction forces at such high sliding speeds start to behave very differently from what is commonly observed at low speeds, below cm/s [1, 2]. Large amplitude oscillatory (i.e., sinusoidal) friction forces F now appear that span both sides of the $F = 0$ axis, with an amplitude ΔF greater than the mean friction force $\langle F \rangle$. Expressed in terms of the energy, during "resonance friction" energy put into the system, i.e. work done, now goes into vibrational energy $W_{vib} \sim \Delta F^2$ per oscillation, as well as the mean friction force $W_{slide} \sim \langle F \rangle \Delta x$ per distance Δx travelled (assuming that the effective F never goes below zero). These mechanical vibrations are referred commonly to as "shudder", "chatter", or "bounce" in several types of industries, and are often treated as instabilities. Here, we focus on clutch systems, which appear to display all the main features that are commonly observed in other systems at high sliding speeds.

A clutch is a mechanical system designed to transmit a driving force or torque to another mechanism, typically by physically connecting an initially stationary "*driven*" shaft to a rotating "*driving*" shaft. In the vehicle industry, clutches generally consist of two stacks of interleaved disks, one stack associated with each shaft, that when

X. Banquy · N. Belman · Y. Min · J. N. Israelachvili (✉)
Department of Chemical Engineering, University of California, Santa Barbara, CA 93106, USA
e-mail: Jacob@engineering.ucsb.edu

D. D. Lowrey · J. N. Israelachvili
Materials Department, University of California, Santa Barbara, CA 93106, USA

G. Mordukhovich
Research & Development, General Motors Company, 30500 Mound Road, Warren, MI 48090-9055, USA

engaged press tightly together under spring or hydraulic loading. Successful clutch engagement quickly and smoothly accelerates the driven shaft to the desired speed (and therefore torque). Engaging the clutch abruptly when the engine is turning at high speed is known to cause a jerky start, known as shudder, which is both uncomfortable as well as contributing to long term damage of the clutch itself [7]. In wet clutches, shudder has been associated with stick–slip instability [5]. Indeed, transmission fluids that exhibit shear thinning—a negative slope in the friction force-shearing velocity (F–V) curve—are known to facilitate the development of both stick–slip (characterized by small amplitude saw-tooth spikes) and shudder (characterized by large amplitude sinusoidal oscillations) [8–10] and see Fig. 12 of [5]. Research efforts focusing on new clutch fluid formulations have, therefore, aimed at improving anti-shudder performance [8].

But the properties of the fluid lubricant are not the only ones that lead to the tribological instabilities that result in stick–slip or shudder. Of equal or greater importance is the mechanical inertia (mass and stiffness) and stability of the whole clutch system, i.e., all the components involved in both the driving, driven, and transmitting (connecting) parts. Since clutch systems (as well as brake systems, engines, and many other mechanically powered devices) are composed of different rotating or linearly translating/reciprocating parts moving at very high speeds, with rapid acceleration and deceleration in between, various mechanical resonances of different parts of the system can be excited at different stages of loading, acceleration, and deceleration. These are expected to occur at the various characteristic or resonance frequencies of the system including their harmonic and sub-harmonics, hence the more general term “resonance friction”.

We recently developed a new attachment to the SFA for studying the frictional properties of real life friction materials and lubricating fluids in a pin-on-disk configuration at sliding speeds up to 25 m/s, and have used this new experimental setup to study the frictional behavior of two friction materials and two lubricating oils in order to correlate their respective properties with the main characteristics of shudder.

2 Materials and Methods

2.1 High-Speed Friction Force Measurement in the Surface Forces Apparatus (SFA)

We used a recently developed high-speed tribometer attachment to the SFA 2000 [5, 11] for measuring friction forces (and surface temperature changes) at high sliding speeds. This attachment uses the pin-on-disk geometry which is commonly used in tribology research. An equivalent mechanical circuit of the tribometer is shown in Fig. 1. The lower surface is a sapphire disk of diameter 3.8 cm which can be rotated by an electrically commuted (EC) motor (EC 20 at 3 W, Maxon Precision Motors, Inc., MA) at linear speeds ranging from 5 to 25 m/s. The disk is mounted with spring clips that hold the disk to the motor while several positioning screws tilt the disk in two axes, enabling rotation that is flat to within* 10 μm per revolution. The loading mount (Applied load in Fig. 1) consists of a double cantilever spring of known stiffness K_L, fitted with strain gauges to allow continuous monitoring of the load, L. The friction forces F are measured with strain gauges attached to another double cantilever spring of known stiffness K_F, as in previous devices [12]. The upper (nominally stationary) and moving surfaces are shown schematically by the masses m and M in Fig. 1. The natural (resonance) frequency of the loading mass was

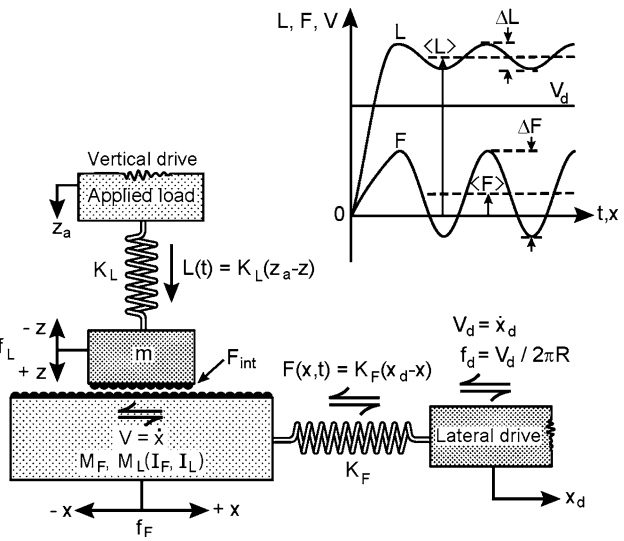

Fig. 1 Schematic mechanical circuit of the experimental setup used in the Surface Forces Apparatus (SFA) in this study (see [5] for details). Sliding motion between the two inertial masses M and m is generated by a motor drive running at a controlled speed V_d. This moves mass M (of inertia I) at a sliding speed V relative to mass m. Note that it is the same as V_d only during steady-state motion or “smooth” sliding but is different during “intermittent”, such as stick–slip or oscillatory (shudder), motion, and in the presence of large transient forces, as can occur at rapid start-up and/or slow-down. A cantilever spring of stiffness K_F measures the friction force $F(x, t)$, which is the same as the actual friction force F_{int} acting at the interface between the two surfaces only in the case of smooth sliding. The measured friction force F may thus vary in a complex way with time t and the sliding distance x (*inset*), even at constant normal load L and driving speed V_d. A spring of stiffness K_L applies the load L to the upper surface of mass m through the controlled displacement z_a of a vertical drive. Due to surface features (e.g., roughness, tilt), inertial effects, and nonlinearities in the horizontal back-and-forth or rotational drive motion, the measured load can also vary intermittently with x and t, which is in turn coupled to the variation in F. Thus, complex time and displacement-dependent fluctuations can occur in both F and L

f_L^0 & 38 Hz (in the normal, z-direction), and that of the friction mass M was f_F^0 & 360 Hz (in the lateral, x-direction), as shown in Fig. 1. These values varied by ± 10% from one experiment to another due to variations in M, m, and the experimental settings.

We may note (i) that *at any instant* or time t the driving velocity V_d is not necessarily the same as the velocity (V or V_{int}) of the surfaces relative to each other at the shearing interface, (ii) that the *measured* friction force, $F(x, t)$, is not the same as the friction force between the surfaces at the shearing interface, F_{int}, and (iii) that even when the position z_a of the loading mount is fixed, the *measured* load itself may vary if z changes during rotational sliding, e.g. due to dynamic effects or surface features. As described in [5], thermocouples were also placed within the friction material (see below). High-speed data sampling ($>2.5 \times 10^3$ samples/s) was performed using a digital oscilloscope (Tektronik model DPO3000).

The modified surface forces apparatus developed for this study was capable of sliding speeds of 5–25 m/s (40–175 rps) and loads up to * 1 N, corresponding to pressures of * 1 MPa (based on post-test visible contact areas * 1 mm in diameter). Higher pressures are possible when measuring transient loads and harder materials, and are limited by the axial load tolerance of the motor. During experiments, the following parameters were measured using the digital oscilloscope (Tektronik model DPO3000): the "measured" friction force $F(x,t)$ as sensed by the horizontal spring in Fig. 1, the "measured" load $L(x,t)$ as sensed by the vertical spring in Fig. 1, and the rotational frequency f_d sensed by electric commutation of the motor (from which we calculate the rotational speed $V_d = 2\pi R f_d$). From these values, we calculated the time-averaged (over 1 s) mean friction force $\langle F \rangle$, the amplitude of the friction force oscillations ΔF, the average load $\langle L \rangle$, the load amplitude ΔL, and transient behavior such as shudder build up and decay.

2.2 Friction Materials and Lubricating Oils

Two friction materials and two lubricating oils were tested in this study. These materials were chosen due to their wide use in the automotive industry in clutch systems. Annular clutch plates (fibrous friction material resin bonded to a metal backing plate) were machined to obtain a round disk with a diameter of 1 cm and an exposed friction-material surface curved to a radius of 5 cm. A small hole was drilled through the metal backing plate of the friction material in order to place small thermocouple wires (type K) as close as possible to that surface, i.e., within the friction material without affecting any of its thermo-mechanical properties. In addition to the temperature of the junction, the temperature of the rotating disk before and after contact were measured separately using IR temperature sensors (type K) focused on the rotating disk immediately before and after the point of contact to measure some mean (locally averaged) temperature change occurring at the shearing junction. All temperature data were recorded using a National Instruments 9219 data acquisition module and LabView SignalExpress software.

Table 1 Physical and chemical properties of the two friction materials and oils studied

Properties	Friction materials (surfaces)		Oils (ATFs)	
	Orange	Green	DX6 (DEXRON -VI)	DCT
Physical	Less dense fibers (10–30 μm in diameter)	Dense synthetic fibers (1–3 μm in diameter forming bundles)	Viscosity (Pa.s)/Shear rate (s^{-1}) @ 40 C	
			0.0286/10	0.0314/10
			0.2712/100	0.0317/100
	Inorganic fillers (0.3–1 μm diameter)	Inorganic fillers (2–5 μm diameter)	Flash point (C)	
			220	>85
	Soft polymer binder (orange color)	Soft polymer binder (green color)	Density (kg/l) @ 25 C	
			0.85	0.86
Chemical	Cellulose-based fibers	Carbon-based fibers		

The first friction material, henceforth called the "orange" friction material, was a traditional resin-bonded *cellulose-based composite* material used in automotive wet clutch applications [13, 14]. The second friction material, called the "green" friction material, was a modern *carbon-and-aramid-fiber-based composite* material used in automotive wet clutch applications. Both friction materials also contained inorganic fillers and proprietary components to provide structure, control friction, and limit wear. The two lubricating oils were fully formulated automatic transmission fluids (ATF). The first oil DEXRON -VI, also called DX6 in the text, is current state-of-the art. The second oil, called DCT, is under development for use in advanced clutch applications. Table 1 summarizes the main physical characteristics and chemical properties of the two friction materials and oils used in this study.

2.3 Physico-Chemical Analysis

Friction materials samples were imaged before and after the tribotests by scanning electron microscopy (SEM, Geol XL30). Chemical analysis of the materials before and after

the tests was performed using a Kratos Axis Ultra X-ray photon electron spectroscopy (XPS) system.

3 Results

3.1 Observation of Resonance Friction (Shudder)

Figure 2 shows an example of the F-L-f_d data collected during an experiment. The load, L, and friction force, F, are characterized by their mean values, $\langle X \rangle$, together with an amplitude ΔX whose dominant oscillatory frequency depended (in addition to the friction material and oil) on the rotational frequency, f_d (which is related to the sliding or shearing velocity by $V_d = 2\pi R f_d$) in relation to the resonance frequencies of the load and friction-measuring components of the device, f_L and f_F, a quality or damping factor, Q_L and Q_F, and resonance response time constants, τ_L and τ_F, all of which together also determine the times to enter and exit resonance, τ_{in} and τ_{out}, and the "stability" of shudder under steady-state driving conditions (f_d = constant), described later. The results and trends observed are qualitatively similar to those previously reported [5] using the extended bimorph slider and model surfaces (sapphire, silica, and surfactant-coated mica) and oils (simple hydrocarbon liquids), indicating that they are not device, surface or lubricant-specific.

Depending on the applied rotational speed and load, and L, resonances can occur in either the load or the friction forces, manifested by a large increase of the signal amplitude as indicated by II (load resonance) and III (friction resonance) in Fig. 2. Type I response in Fig. 2 is when there is no resonance in either the load or friction forces. Figure 3 shows expanded views of the data corresponding to these three types of responses.

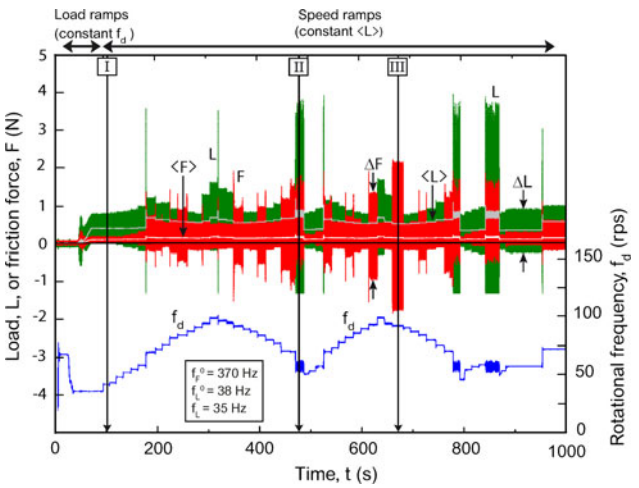

Fig. 2 Condensed view of the three measured parameters, F, L, and f_d as a function of time t obtained from an experiment involving the green friction material and DCT oil (the load L in green, rotational frequency f_d in *blue*, and friction force F in *red*)

Figure 3a (type I—no resonance or shudder) represents a situation where the load L and friction force F are oscillating in phase, both at a small amplitude and at the frequency of the rotational frequency, f_d (= 30 rps). The observed oscillations in L and F are here due to unavoidable imperfections in the mechanical system or surfaces, for example, imperfect alignment of the rotating disk, which is reflected in the oscillations in L and in turn cause oscillations in F, all at the same frequency.

Figure 3b shows an example of type II resonance response in the load–load shudder. The load exhibits large amplitude oscillations which in turn induce oscillations in F at the same frequency.

Figure 3C shows an example of resonant friction (friction shudder) where F is oscillating at a frequency much higher than the driving speed. The frequency of F during this event is equal to the natural resonant frequency of the friction measurement device, f_F^0 (≈ 370 Hz) while the main frequency of the load trace equals the rotational frequency, f_d.

It is important to note that, due to the complex fibrous/porous nature of the friction materials used, it is not possible to measure or even define the lubricant "film thickness" or "real contact area" in such systems, as also concluded by Ingram et al. [16].

Figure 4 represents the short-time Fourier transform (STFT) of F and L. It is readily seen that the frequency associated with the first (principal) harmonic of the friction force or the load at the beginning of the experimental run ($t < 100$ s) is equal to the rotational frequency, f_d (in rps units). However, during a shudder event (II and/or III), the principal harmonics have frequencies that are now close to the natural frequency of the friction device or loading mass which determine the frequencies of the shudder—the intensities being determined by additional factors such as the inertia and tribological properties of the device (friction material, lubricant fluid, etc.).

3.2 Occurrence and Intensity of Shudder

The occurrence of a shudder event is determined by the resonance frequencies of the loading system and the friction measurement device. Figure 5 shows the evolution of the friction force amplitude, ΔF, as a function of the rotational speed for both friction materials and lubricating fluids. In each case, a sharp increase in ΔF, i.e. a shudder event, occurs at a rotational frequency, f_d, corresponding to a multiple or fraction of the uncoupled resonant frequency of the friction device, f_F^0 or the coupled resonant frequency of the loading device, f_L. The intensity of the shudder event

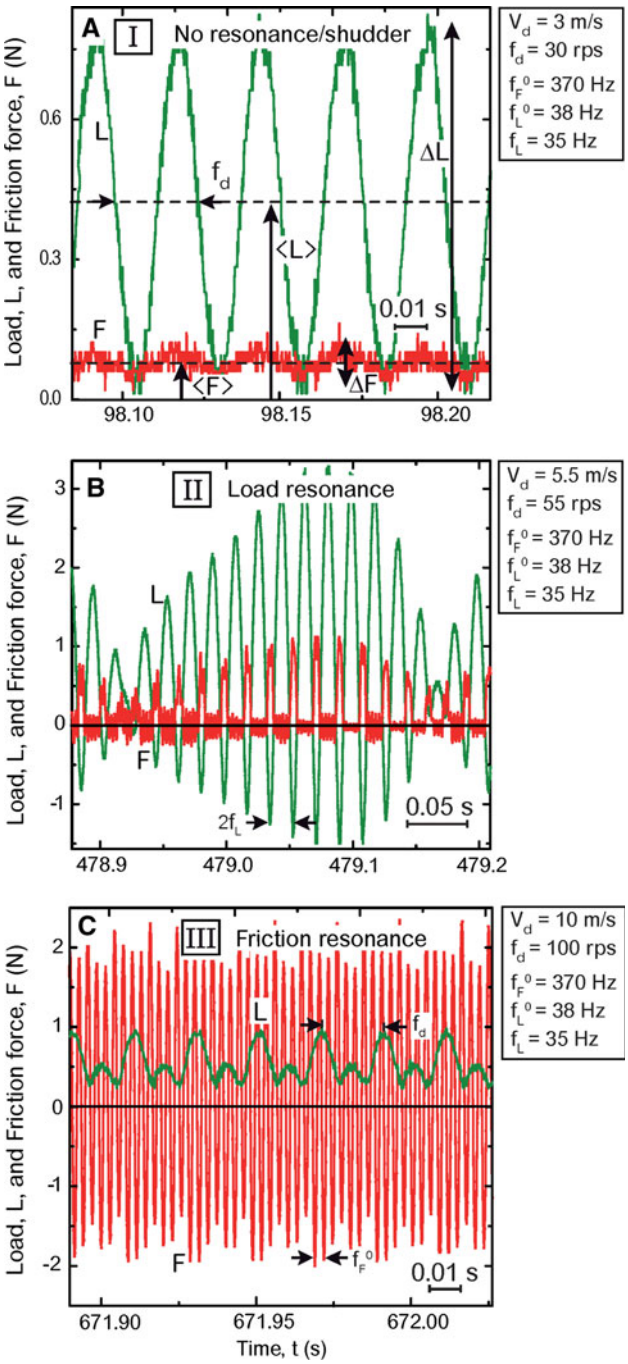

Fig. 3 Ampli ed views at selected instants (I, II, and III) of the results shown in Fig. 2. These experimental data illustrate the different types of friction regimes (no shudder—type I, friction shudder—type II, and load shudder—type III) that manifest themselves at three selected moments in time. The onset of shudder—the "shudder event" is characterized by a large increase in the force amplitude (load shudder II, and friction shudder I, II, *panels B and C*), compared to no or little shudder in either the friction force F or the load L (*panel A*)

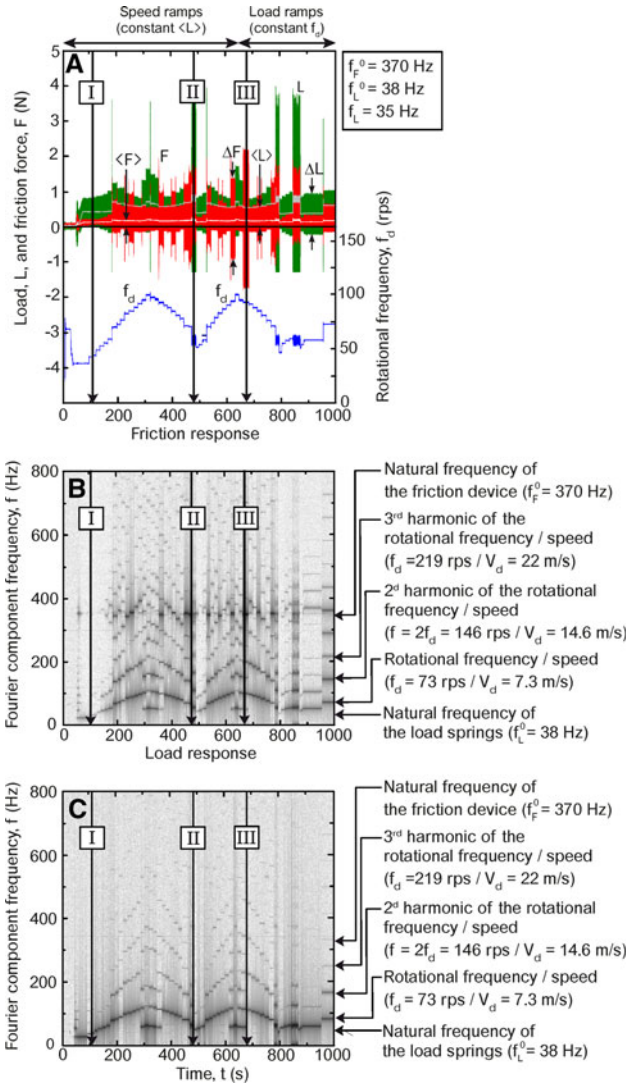

Fig. 4 b and c The short-time Fourier transforms (STFT) of the friction force F and load L obtained from the data represented in *panel A* and Fig. 2. For each time interval (* 0.5 s), the relative intensity of the Fourier component associated to a given frequency may be seen by the color saturation at that point. This representation allows the display of the frequency and amplitude associated with each harmonic of the FT of the load and friction force trace as a function of time

assessed by ΔF depends on the nature of the lubricating fluid more than the friction material. Indeed, experiments performed with DCT oil systematically exhibit very intense ΔF peaks compared to DX6-lubricated surfaces. This last point is correlated to the fact that DCT-lubricated surfaces have a higher friction coefficient than DX6-lubricated surfaces. As shown in Fig. 6, the oil dominated over the friction material in determining the friction coefficient in the range of load studied (which corresponds to nominal mean pressures P * 0.1–1 MPa given by $P = \langle L \rangle / S$ = mean load/apparent contact area, where S is imaged after the experiments (see Fig. 9). The medium to high friction coefficients of μ * 0.2 seen with DCT are close to those seen between poorly lubricated solids while those with DX6 of μ * 0.04 are typical of well-lubricated surfaces.

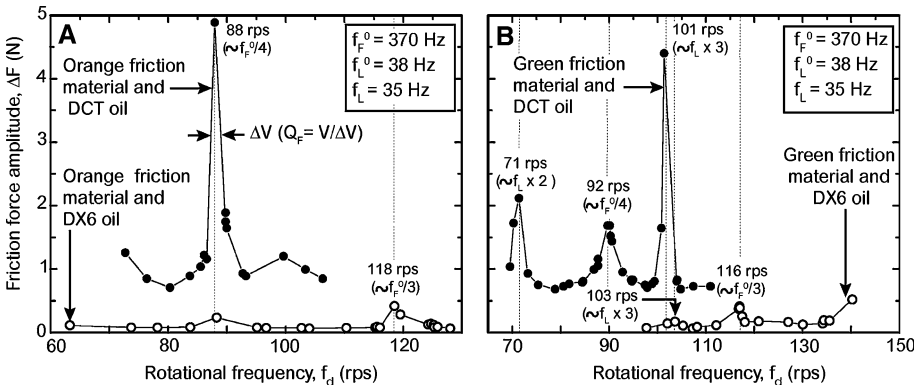

Fig. 5 Evolution of the friction force amplitude ΔF as a function of the rotational frequency for the *orange* friction material (a) and the *green* friction material (b). Each material was tested with both lubricating fluids, DCT and DX6, as shown

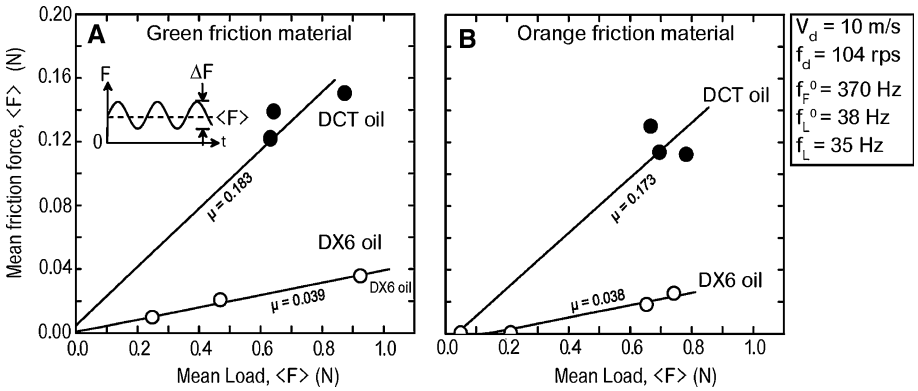

Fig. 6 Mean friction force $\langle F \rangle$ versus applied load L for the a *orange* and b *green* friction materials with DX6 fluid (*filled circle*) and DCT (*open circle*) friction fluids at a rotational frequency of $f_d = 104 \pm 1$ rps

3.3 Distinctions Between "Load Shudder" and "Friction Shudder"

Figure 7 represents single-time FFT spectra of the friction force F extracted from the STFT shown in Fig. 4 for the frictional system of sapphire against the green friction material in DX6 oil. The black trace in Fig. 7a shows that at a rotational frequency of $f_d = 126$ rps and a load of $L = 0.9$ N the existed frequencies during sliding (type in Fig. 2) are limited to f_d, $2f_d$, and $3f_d$. If the same system is loaded in a state of load shudder (type, red trace) at the same rotational frequency but $L = 0.5$ N, the dominant frequencies now become 63.5 rps ½ $f_d = 2f_L$, with additional frequencies evident at multiples of f_L. Additionally, the friction device uncoupled resonant frequency $f_F^0 = 360$ rps is also excited, even though its frequency does not match the rotational excitation. This is a general property observed in this system, viz. that load shudder induces friction shudder.

The differences between friction shudder (type, black trace) and load shudder (type, red trace) are readily apparent for constant $L = 0.5$ N at $f_d = 120$ rps (Fig. 7b). The responses at $f_d = f_F^0$ are of the same magnitude and frequency, but the friction shudder response displays a higher damping factor Q than the load shudder. Other than this large response at f_F^0, the friction shudder response is not qualitatively different from the no-shudder case. The load shudder response is similar to the response in Fig. 7a with the additional feature that now multiples or fractions of f_d coincide with both f_F^0 and f_L. Also, whereas the ½ f_d peak has shifted with the change in speed, f_L remains stable within a narrow range.

In Fig. 7c, the shudder friction response data at $f_d = 118$ rps and $L = 0.5$ N from Fig. 7b is reproduced, with the addition of the responses at $L = 0.9$ and 0.2 N. The peaks do not move relative to the $L = 0.5$ N case, indicating a weak or no load effect on the response frequency of the friction device. We may note, however, that the increased load L does further increase the Q_F of the friction device response (shown in blue). Conversely, a low average load such as 0.2 N results in a lower Q_F in the friction device response, similar to the Q_L value seen during load shudder.

3.4 Development, Transient Effects, and Decay of Shudder

Figure 8a shows characteristic friction force and load traces for the development and decay of friction shudder without load shudder. The system shown is the orange friction material and DCT fluid at $\langle L \rangle = 0.3$ N, $T = 32$ °C, but the qualitative behavior does not significantly vary for

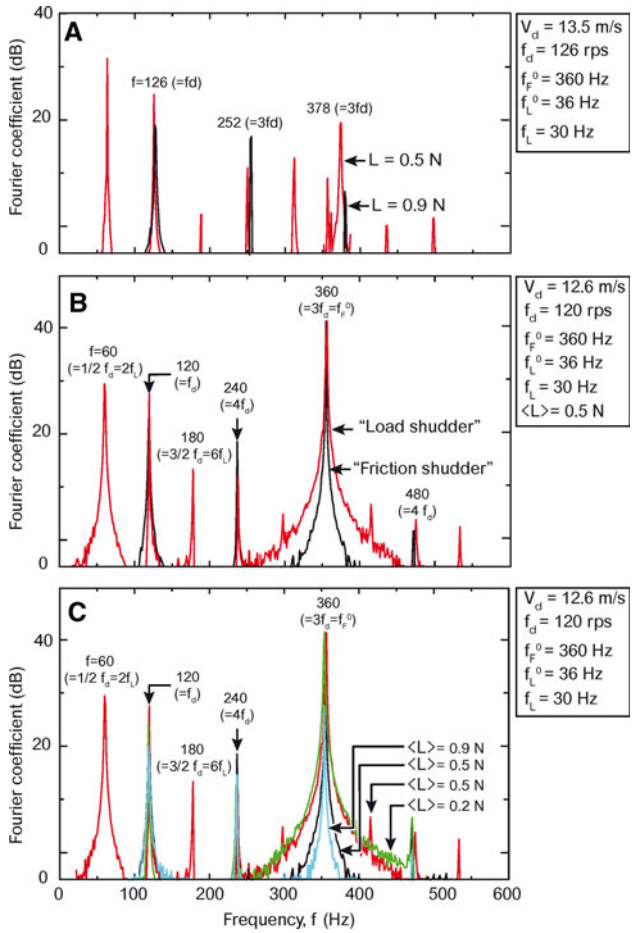

Fig. 7 Single-time FFT spectra of the friction force F extracted from the STFT shown in Fig. 4 for the frictional system of sapphire against the *green* friction material in DX6 oil. a Purely sliding conditions. *black line* ($L = 0.9$ N), load shudder conditions: *red line* ($L = 0.5$ N). b Differences between friction shudder (*black trace*) and load shudder (*red trace*) observed in the FFT at constant $L = 0.5$ N and $f_d = 120$ rps. c The shudder friction response data at 120 rps and 0.5 N from *panel b* is reproduced, with the addition of the responses at 0.9 and 0.2 N. The results show that an increase in load increases the Q of the friction device response (*shown in blue*)

the other systems studied. Initially, the rotational speed is at a non-shudder value. As the speed is increased, the motor transiently goes through a shudder frequency and overshoots before settling at the shudder frequency of $f_F^0 = 4f_d$ in this case. We may note that the growth of shudder is slower than its decay, which occurs over a period comparable to the (characteristic relaxation) time constant of the friction device, $\tau_F \approx 0.075$ s.

Development of load shudder and cyclically induced friction shudder depends on the rotational speeds and, τ_d, but not on the large time constant of the load spring, $\tau_L \approx 1$ s (see Fig. 8b, the system shown is the orange friction material and DX6 fluid at $\langle L \rangle = 0.7$ N, $T = 33$ °C). Load shudder induces transient friction shudder when a multiple of the rotational speed is close enough to f_F^0 such that the free oscillations of the friction device in between the high-load point interact constructively with the friction force spikes, developing into a shudder state where free oscillations of the friction device are of comparable magnitude to the friction force spikes (Fig. 8c). Since the match is not perfect, the shudder is not stable and eventually decays. The system is green friction material and DX6 fluid at $\langle L \rangle = 0.6$ N, $T = 26$ °C. Large variation in load L as observed during load shudder is also possible without friction shudder (Fig. 8d, the system is green friction material and DCT fluid at $\langle L \rangle = 0.7$ N, $T = 30$ °C). The measured friction force and load are 90° out of phase due to the location of the load measurement.

3.5 Thermal Effects

The measured temperature rise ΔT in the contact during an experiment was always small (a few degrees Celsius), and primarily reflected heat transfer from the warmer lower disk to the cooler friction material. The temperature rise measurement is constrained by the volume sampled by the thermocouple; for a system of this kind the temperature rise due to friction is expected to be only on the order of 0.5 °C. Higher loads (pressures) enhanced the heat transfer from the lower surface to the upper surface, generally increasing the temperature (results not shown).

3.6 Chemical Analysis of the Friction Materials

Black shiny spots of *glaze* of ≈ 1 mm in diameter were observed in the center of the friction materials after friction experiments with DX6 and DCT fluids, using optical microscopy. For example, Fig. 9a, b shows optical microscopy images of the orange friction material before and after the tribological experiment, respectively, with DX6 oil. The glaze area is marked with a circle in Fig. 9b. SEM images present the above-mentioned friction material before and after the tribological experiment (Fig. 9d, e, respectively), in the contact area. Polishing of the contact area can be clearly observed in Fig. 9e. In addition, Fig. 9f shows SEM image observed outside the contact area, which is similar to the untested sample (Fig. 9d), since it was not polished. After this friction experiment (Fig. 9b, c), the DX6 oil was washed away with Petroleum Ether. As can be seen in Fig. 9c, the glaze is still present in the sample confirming that its origin is due to a change in the surface morphology. The chemical analysis of the glaze formation was done using XPS. The glaze composition could not be identified, since this method is a surface-sensitive method and residual oil covered the sample (fibers) including the glaze, as can be seen from Table 2. Hence, we compare the chemical composition of the untested friction material without oil to the samples after

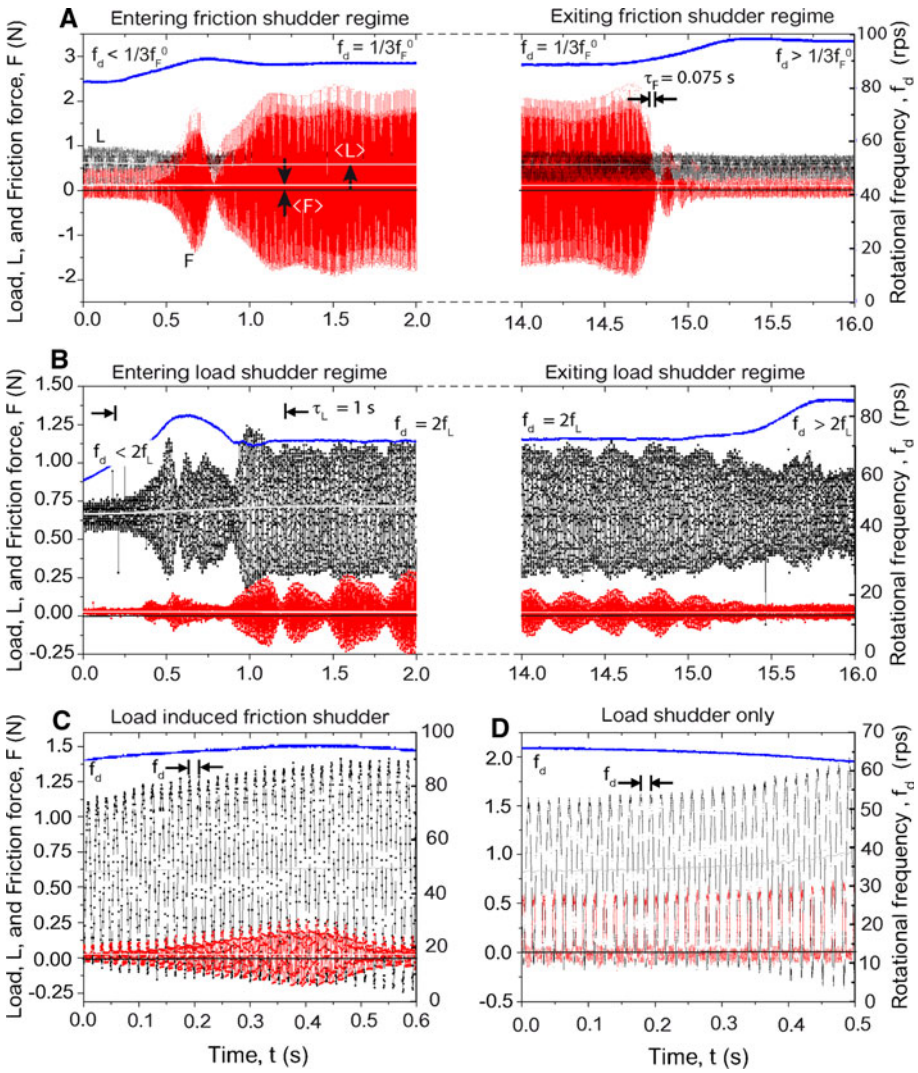

Fig. 8 a Characteristic friction force and load traces during shudder development and decay for the *orange* friction material and DCT fluid at $\langle L \rangle = 0.3$ N, $T = 32$ °C. b Development and decay of load shudder for the orange friction material and DX6 fluid at $\langle L \rangle = 0.7$ N, $T = 33$ °C. c Friction force and load traces for the green friction material and DX6 fluid at $\langle L \rangle = 0.6$ N, $T = 26$ °C showing transient friction shudder induced by load shudder when a multiple of the rotational speed is close to f_0 but not enough to evolve into stable shudder. d Load and friction force traces showing that load shudder characterized by a large amplitude of the load trace is possible without friction shudder. The system is green friction material and DCT fluid at $\langle L \rangle = 0.7$ N, $T = 30$ °C

running the friction experiment with DX6 oil (containing glaze in the contact area—see Fig. 9b) and washing the oil away with petroleum ether (Fig. 9c). The chemical composition of the friction material surface in the contact area (including the glaze which remained) was very similar to the as-received sample (Table 2), indicating that the glaze was formed only due to the morphological change of the surface. The same phenomenon was observed with the green friction material and DX6 oil (Table 2). Therefore, mechanical fiber polishing and burying of the fibers in the resin are identified as the primary reason for the friction material darkening.

4 Discussion and Conclusions

4.1 Origin and Nature of Shudder

From our experiments using the HS-SFA, we conclude that shudder is characterized by an *oscillatory* friction force (as opposed to sharp *stick–slip* friction spikes). Load shudder is likewise manifested by oscillations in the effective load, due to mechanical displacements, even when the nominal (applied) load is fixed. In general, shudder can be more completely characterized in terms of its magnitude, frequency, stability, Q value, development, and decay times.

4.2 When Does Shudder Occur and at What Frequencies

We conclude that shudder occurs at and when one of the Fourier (*frequency*) components of the mechanical system (either in the normal, load, or lateral, friction, directions) coincides with the rps (revolution frequency) of the rotating disk. However, the *mean* friction force, $\langle F \rangle$, and *intensity* of shudder (friction amplitude, ΔF) depend on other factors, described later.

The natural resonance frequencies of the mechanical system, which are related to the inertia and elasticity of the

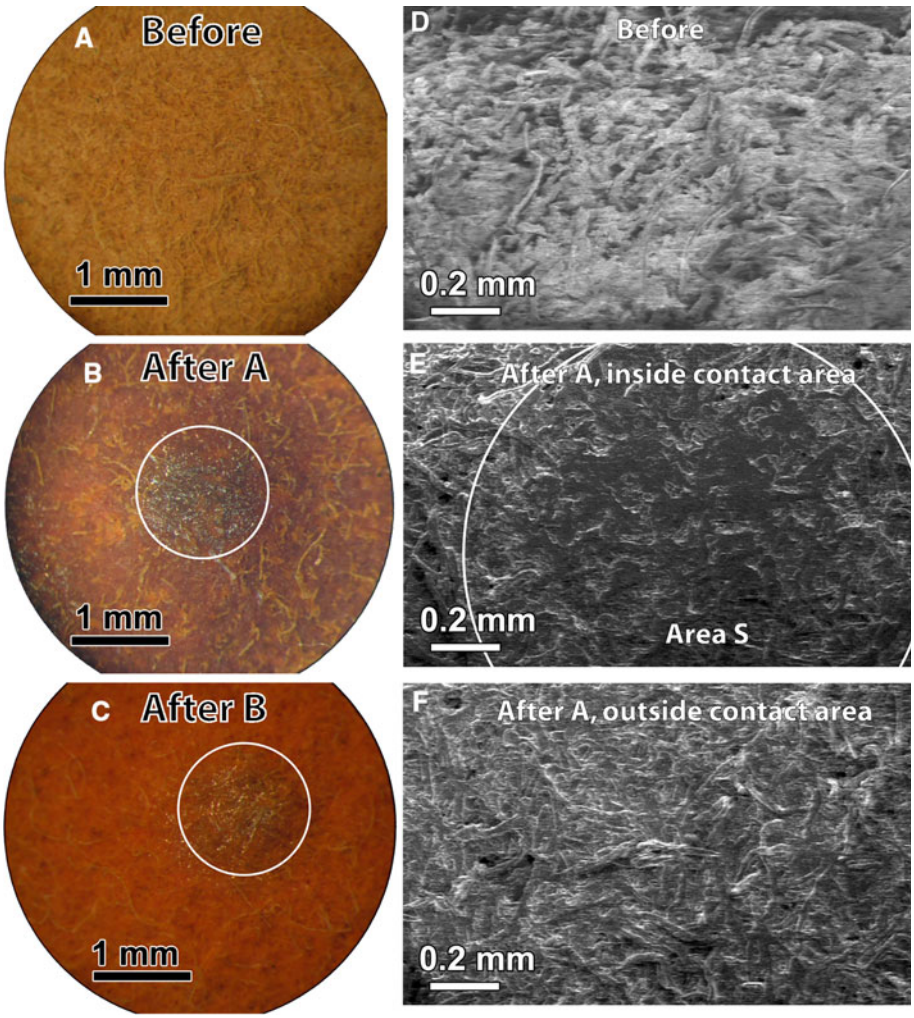

Fig. 9 a–c Optical microscope images of the orange friction materials before (as received) and after friction tests, and inside and outside the contact areas (*shown by circles*). a As received, b after friction experiments with DX6 oil, and c same as b after washing away the oil with petroleum ether. The contact areas in a and b are visibly darker, and small white crystals that were nucleated or deposited (trapped) in the contact are also observable. d–f SEM images of the orange friction material (d) as received (without oil, prior to a friction experiment) show a surface that is very rough on the micro-scale. e–f SEM images of the orange friction material after friction experiments with DCT oil (e) inside and f outside the contact area show that the contact area has been polished, leaving a smoother area with fewer fibers. This polishing may account for the visual darkening of the friction material. The results of XPS chemical analysis of the different friction materials and their surfaces are given in Table 2

device elements, are critical for the system's frequency response. These resonant frequencies determine what sort of shudder behavior is possible. Friction shudder occurs when the rotational frequency, or one of its multiples, is close enough to the *uncoupled* resonant frequency of the friction device, f_F^0. On the other hand, load shudder occurs when the rotational frequency, or one of its multiples or natural fractions, is close to the *coupled* resonant frequency of the loading device, f_L. Load shudder induces transient friction shudder when a multiple of the rotational speed is close enough to the coupled frequency of the load device, f_L, due to the tribological coupling between friction and load.

4.3 Effect of Friction Material and Lubricating Oil on Resonance Friction Characteristics (Intensity, Amplitude, etc.)

Our results showing greater friction force amplitude ΔF for DCT fluid irrespective of the friction material are supported by Cavdar and Lam [15], who report that high VI fluids may behave more "stiffy" than expected due to the difficulty that highly branched polymers have in flowing into small pores. At the other end of the spectrum (e.g. hexadecane), small molecules can order in confined spaces, effectively freezing and so increasing the system stiffness through a different route.

The differences between DX6 and DCT show the importance of surfactants on friction system behavior. Both fluids are mineral oil-based automatic transmission fluids (ATF) with DCT having higher viscosity and higher oxygen content (~ 9 vs. 5%) as seen on Table 2.

The effect of the fluid and material combination on the available speed/load range as well as the analog speed control limited the variability of data on shudder development. Thus, the quality and quantity of time to shudder data is not ideal. Trends are inconsistent, but there does seem to be a tendency for DCT oil samples to have a longer time to develop quasi-stable shudder. The more readily apparent factor influencing time to shudder was the driving velocity. Longer times to shudder may be associated with sliding speeds that do not match a device-critical

Table 2 Results of XPS analyses of green and orange friction materials (brous resin bonded to steel metal backing plates) with DX6 and DCT oils

Friction material	Friction oil	Condition of assay	Position related to contact area	Atomic number density[%]			
				C 1s	O 1s	Si 2p	N 1s
None	DX6	As received	NA	91.7	4.8	3.5	0.0
	DCT		NA	85.9	9.1	5.0	0.0
Green	None[b]	As received	NA	80.0	15.0	1.1	3.9
	DX6	Friction tested	Outside	93.2	4.6	2.2	0.0
			Inside	93.5	4.0	1.9	0.6
		Friction tested + washed	Outside	85.2	11.1	1.5	2.2
			Inside	86.9	9.8	1.3	2.0
	DCT	Friction tested	Outside	87.6	7.5	4.9	0.0
			Inside	85.7	9.2	5.1	0.0
Orange	None[b]	As received	NA	80.4	17.1	1.2	1.3
	DX6	Friction tested	Outside	92.3	4.9	2.8	0.0
			Inside	92.5	4.8	2.7	0.0
		Friction tested + washed	Outside	87.7	11.7	0.2	0.4
			Inside	90.8	8.8	0.2	0.2

The friction materials were analyzed with and without the oils, before and after the friction experiments. In addition, the friction materials were analyzed after washing away DX6 oil with petroleum ether. Optical microscope and SEM images of these samples are shown in Fig. 9

[a] The glaze composition could not be identi ed using XPS since is a surface-sensitive method and residual oil covered the sample (bers) including the glaze. After running the friction experiment with DX6 oil (containing glaze in the contact area—see Fig. 9) and washing the oil away with petroleum ether, the chemical composition of the friction material surface in the contact area (including the glaze which remained) was very similar to the as-received sample

[b] No lubricating oil was present on the friction material during the chemical analysis

frequency, but are close enough to cause shudder. Shudder decay was more general and tied to the characteristic relaxation time of the friction device.

4.4 Chemical and Physical (Structural) Changes of the Surfaces-Induced by Resonance Friction

Pressures on the order of 1–10 MPa are expected to result in a compression of perhaps 50 μm in the friction material. SEM imaging of the friction materials shows that this displacement is on the order of the diameter of a single ber, and thus at full load the real area of contact between the friction material and facing plate is a very small percentage of the total apparent area of contact [16, 17]. The frictional behavior of the engaged clutch under slip will be dominated by the tribopair of bers in the friction material versus the facing material under boundary lubrication conditions. Since the bers stick out from the surface, they will tend to quickly break through any bulk liquid lm so the conventional description of a lm thickness does not apply [16]. The surrounding lubricant that lls in the space between the two surfaces will support a small fraction of the load, mostly upon initial loading, and may be thought of as a continuous layer that heats slightly due to shearing and conducts heat from the facing plate.

In our characterization of the friction material, we have demonstrated (using XPS) that the glaze in our system is most probably formed due to *morphological* changes of the surface ("polishing") rather then chemical changes or formation of a new phase. Especially, as was shown by the XPS analyses (Table 2), after friction experiment with DX6 uid (with glaze observed in the center of the sample) and washing the uid away with Petroleum Ether, the chemical composition of the sample in the center (the glaze) was the same as of the friction material without uid. Glaze presence after washing away the uid was also evident from the optical microscope image (Fig. 9), and hence supports the conclusion that the glaze we observed represents a morphological change of the friction material.

5 Concluding Remarks

The tribological behavior of model automotive friction surfaces lubricated with ATFs using a new high-speed attachment to the SFA that allows for friction measurements to be made at sliding velocities up to 20 m/s reveals that at sliding velocities above * 1 cm/s or reciprocating/rotational frequencies above 200 rps (Hz), depending on the system, new friction and load responses appear, characterized by large amplitude oscillations that are quite

different from stick–slip motion. These oscillations arise from the "resonant coupling" between the different moving mechanical parts of the system. Our results and trends observed are qualitatively similar to those previously reported [5] using different attachments, model surfaces, and oils, indicating that they are not device, surface, or lubricant-specific. We conclude that resonance friction depends only indirectly on the purely frictional properties of the shearing interface, such as the coefficient of friction, but directly on the loading and sliding directions and speeds, the geometry and inertia (mechanical properties and especially the resonant frequencies) of the moving parts of the whole system, and on any imperfections, defects or misalignments of the connected moving parts. Including these purely mechanical-inertial effects in any tribological model is necessary for fully understanding, designing, or controlling frictional behavior at high speeds or reciprocating/rotational frequencies in machines, clutches, brakes, and hard disk-drives, etc., where "resonance friction" (also referred to as "shudder", "chatter", "bounce", etc.) is commonly observed.

Acknowledgments We thank Mark Kornish for technical assistance for the SEM characterization of the friction materials. SEM and XPS were conducted at CNSI (UCSB). The development of the HS-SFA was supported by the Department of Energy under grant DE-FG02-87ER45331. XB, NB, and DDL were supported by the Department of Energy under the same grant. Friction materials and oils were provided by General Motors Co.

References

1. Mate, M.: Tribology on the Small Scale. A Bottom up Approach to Friction, Lubrication, and Wear. Oxford University Press, Oxford (2007)
2. Friesen T: Chatter in wet brakes. SAE Tech. Pap. Ser. 831318 (1983)
3. Ohtani H, Hartley R, Stinnett D: Prediction of anti-shudder properties of automatic transmission fluids using a modified machine. SAE Tech. Pap. Ser. 940821 (1994)
4. Slough, C.G., Everson, M.P., Jaklevic, R.C., Melotik, D.J., Shen, W.D.: Clutch shudder correlated to ATF degradation through local friction vs. velocity measurements by a scanning force microscope. Tribol. Trans. 39, 609–614 (1996)
5. Lowrey, D.D., Tasaka, K., Kindt, J., Banquy, X., Belman, N., Min, Y et al.: High speed friction measurements using a modified surface forces apparatus (SFA). Trib. Lett. 42, 117–127 (2011)
6. Ostermeyer, G.P.: On the dynamics of the friction coefficient. Wear 254, 852–858 (2003)
7. Ohkawa, S.: Wet clutches and wet brakes for construction equipment and industrial machines. Jpn. J. Tribol. 39, 1439–1450 (1994)
8. Murakami Y: Anti-shudder property of automatic transmission fluids—A study by the international lubricant standardization and approval committee (ILSAC) ATC committee. SAE Tech. Pap. Ser. 2000-01-1870 (2000)
9. Rodgers, J., Haviland, M.: Friction of transmission clutch materials as affected by fluids, additives, and oxydation. SAE Tech. Pap. Ser. 194A 600178 (1960)
10. Watts, R., Nibert, R.: Prediction of low speed clutch shudder in automatic transmissions using the low velocity friction apparatus. In: 7th International Colloquium Tribology, Esslingen, Germany (1990)
11. Israelachvili, J.N., Min, Y., Akbulut, M., Alig, A., Carver, G., Greene, W., et al.: Recent advances in the surface forces apparatus (SFA) technique. Rep. Prog. Phys. 73, 036601 (2010)
12. Israelachvili, J.N.: Measurement and relation between the dynamic and static interactions between surfaces separated by thin liquid and polymer- lms. Pure Appl. Chem. 60, 1473–1478 (1988)
13. Bijwe, J.: Composites as friction materials: Recent developments in non-asbestos fiber reinforced friction materials—A review. Polym. Compos. 18, 378–396 (1997)
14. Kitahara, S., Matsumoto, T.: Present and future trends in wet friction materials. Jpn. J. Tribol. 39, 1451–1459 (1994)
15. Cavdar, B., Lam, R.C.: Wet clutch performance in a mineral-based and in a partial-synthetic-based automatic transmission fluid. Tribol. Trans. 41, 160–169 (1998)
16. Ingram, M., Spikes, H., Noles, J., Watts, R.: Contact properties of a wet clutch friction material. Tribol. Int. 43, 815–821 (2010)
17. Otani, C., Kimura, Y.: Analysis of the real contact area of a paper-based wet friction material. Jpn. J. Tribol. 39, 1487–1494 (1994)